Molecular Dynamics Simulation of a Lipid Diamond Cubic Phase

Siewert-Jan Marrink*,† and D. Peter Tieleman‡

Contribution from the Department of Biophysical Chemistry, University of Groningen, Nijenborgh 4, 9747 AG Groningen, The Netherlands, and Department of Biological Sciences, University of Calgary, 2500 University Drive NW, Calgary, Alberta, Canada T2N 1N4

Received April 12, 2001

Abstract: This paper presents the first atomistic simulation of a cubic membrane phase. Using the molecular dynamics simulation technique both the global and the local organization of glycerolmonoolein molecules inside the diamond cubic phase are studied. Multinanosecond simulations reveal that the center of the cubic bilayer remains close to the infinite periodic minimal surface that describes the diamond geometry. We further show that the equilibrium structure of the surfactant molecules inside the cubic phase is very similar to their structure inside a simulated lamellar bilayer. The small differences arise from the packing constraints of the surfactants within the cubic phase which has an area per surfactant that increases toward the bilayer center.

1. Introduction

The molecular dynamics simulation techique (MD) has been successfully applied to the simulation of surfactant and lipid bilayer systems with atomic detail for over a decade now (for recent reviews see refs 1−3). Many fundamental insights have been obtained from these simulations in terms of organization of the molecules within the bilayer, the complex structure of the bilayer interface, and the dynamical nature of the bilayer on the atomic scale. Apart from micellar systems, nonlamellar systems have thus far received almost no attention with the exception of a hexagonal surfactant phase.[4] The larger system size needed for more complex phases has been prohibitive for such simulations so far. We show that it has recently become feasible to perform realistic simulations of nonlamellar systems. One of the nonlamellar surfactant phases that is of great interest, both from a scientific and from an industrial point of view, is the so-called cubic phase. This phase consists of a highly curved bilayer that is folded in space in such a way as to form a regular pattern of two separated labyrinths of water channels. The cubic surfactant phase has some very specific properties, which explains its growing use in biophysical and biomedical fields and in the food and cosmetics industry. For instance, cubic phases are used to induce membrane protein crystallization (e.g. ref 5), for the controlled release of drugs (e.g. refs 6−8), and as biosensors (e.g. ref 9). Also, cubic-like phases are observed in mitochondria and the endoplasmic reticulum,[10,11] as intermediate structures during many common physiological processes such a cell−cell adhesion and fusion (e.g. refs 12 and 13), and during the digestion process in the stomach (e.g. ref 14). All of the above examples illustrate the use of the specific properties of cubic membranes. However, not much is known about the underlying mechanisms giving rise to these specific properties. Especially on the molecular level insight is experimentally difficult to obtain. Computer simulation studies such as MD can provide insight at the atomic level.

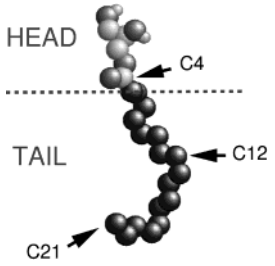

Figure 1. Structure of GMO. Numbering of the carbon positions is indicated for later reference.

We selected the surfactant glycerolmonoolein (GMO) (see Figure 1) for our simulations for two reasons. First, GMO is widely used because it easily forms stable cubic membrane phases. Second, it has a relatively simple structure, which simplifies the simulations. Phase studies[15] show that GMO forms cubic phases when multilamellar stacks are swollen above a water/surfactant ratio of 10−20% (w/w) at a temperature range roughly between 293 and 363 K. At lower temperatures or low water content multilamellar systems are formed whereas at high temperatures inverted hexagonal or fluid isotropic phases are found. Binary surfactant solutions in general can form three different types of bicontinuous cubic phases, the so-called primitive ($Im\bar{3}m$ symmetry), gyroid ($Ia\bar{3}d$ symmetry), and

* Address correspondence to this author. E-mail: marrink@chem.rug.nl. FAX: 31503634800.
† University of Groningen.
‡ University of Calgary.

(1) Tieleman, D. P.; Marrink, S. J.; Berendsen, H. J. C. *Biochim. Biophys. Acta* **1997**, *1331*, 235.
(2) Forrest, L. R.; Sansom, M. S. P. *Curr. Opin. Struct. Biol.* **2000**, *10*, 174.
(3) Feller, S. *Curr. Opin. Colloid Interface Sci.* **2000**, *5*, 218.
(4) Bandyopadhyay, S.; Klein, M. L.; Martyna, G. J.; Tarek, M. *Mol. Phys.* **1998**, *95*, 377.
(5) Rummel, G.; Hardmeyer, A.; Widmer, C.; Chiu, M.; Nollert, P.; Locher, K.; Pedruzzi, I.; Landau, E. *J. Struct. Biol.* **1998**, *121*, 82.
(6) Wyatt, D.; Dorschel, D. *Pharm. Technol.* **1992**, *16*, 116.
(7) Burrows, R.; Collett, J.; Attwood, D. *Int. J. Pharm.* **1994**, *111*, 283.
(8) Chang, C.; Bodmeier, R. *J. Contr. Relat.* **1997**, *46*, 215.
(9) Razumas, V.; Kanapienene, J.; Nylander, T.; Engstrom, S.; Larsson, K. *Anal. Chim. Acta* **1994**, *289*, 155.
(10) Landh, T. *FEBS Lett.* **1995**, *369*, 13.
(11) Luzzati, V. *Curr. Opin. Struct. Biol.* **1997**, *7*, 661.
(12) Siegel, D. *Biophys. J.* **1999**, *76*, 291.
(13) Larsson, K. *J. Phys. Chem.* **1989**, *93*, 7304.
(14) Patton, J.; Carey, M. *Science* **1979**, *204*, 145.
(15) Qiu, H.; Caffrey, M. *Biomaterials* **2000**, *21*, 223.

10.1021/ja016012h CCC: $20.00
Published on Web 11/13/2001

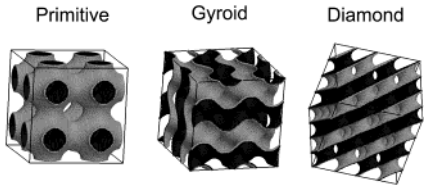

Figure 2. Graphical representation of the three bicontinuous cubic phases (primitive, gyroid, and diamond).

diamond phases ($Pn\bar{3}m$). The geometry of these phases can be described by an infinite periodic minimal surface (IPMS), which is an intersection free (i.e. bicontinuous) triply periodic (i.e. periodic in all three dimensions) surface with an average mean curvature of zero. Figure 2 displays these IPMS for the three different types. Most surfactant−water systems, including GMO, form so-called inverse cubic phases, with the center of the bilayer near the IPMS and each monolayer curving toward the aqueous compartments.[10,16,17] Although the geometry of the primitive phase is the least complicated, GMO only forms gyroid and diamond phases. The size of the cubic phase unit cell depends on the state conditions, with sizes decreasing with temperature and increasing with water content. The unit cell of the diamond phase varies between 7 and 10 nm, whereas for the gyroid phase it varies between 10 and 18 nm. For reasons of computational speed we selected the diamond phase for our simulations, at a low water content of 0.26 (w/w) and fairly high temperature (335 K). The experimental size of the unit cell at these conditions is 7.4 nm.[18] Elevating the temperature further to achieve an even smaller unit cell would technically be possible, but the current force fields are not optimized for such high temperatures.

The current simulations are a first attempt at a detailed understanding of the structure and dynamics of the surfactant and water molecules inside a cubic membrane. Useful insights are obtained from comparison to simulations of GMO molecules in a lamellar phase. Before the results are presented we discuss in some detail the nontrivial way of generating the starting structures of the GMO diamond phase, the several different approaches to obtain a stable cubic phase, and the nonstandard methods of analysis. After the presentation of the results we briefly discuss their implications and propose a model for the packing of the GMO within the diamond phase. We end with a summary of the conclusions.

2. Methods

2.1. Starting Structure. As the exact organization of the surfactants in the cubic cell is not known, we based our starting structure on the general assumption (e.g. refs 10, 16, and 17) that the midplane of the bilayer coincides with the IPMS. The IPMS of the diamond surface (see Figure 2) was first described by Schwarz,[19] and can be closely and most easily approximated by a trigonometric expression,[20] which for the diamond phase reads

$$\sin x \sin y \sin z + \sin x \cos y \cos z + \cos x \sin y \cos z + \cos x \cos y \sin z = C \quad (1)$$

With $\{x, y, z\} \in [0, \pi]$ one unit cell of the diamond phase is described. Although eq 1 strictly speaking is not a minimal surface, the difference is only of mathematical significance. Figure 3 shows one unit cell of the approximated minimal surface according to eq 1. Via simple symmetry operations the whole diamond unit cell can be constructed from 24 asymmetric units, the so-called flächenstücke. The six surface pieces indicated in Figure 3 consist of four of these flächenstücke each. One of these surface pieces is used as a building block to generate our starting configuration.

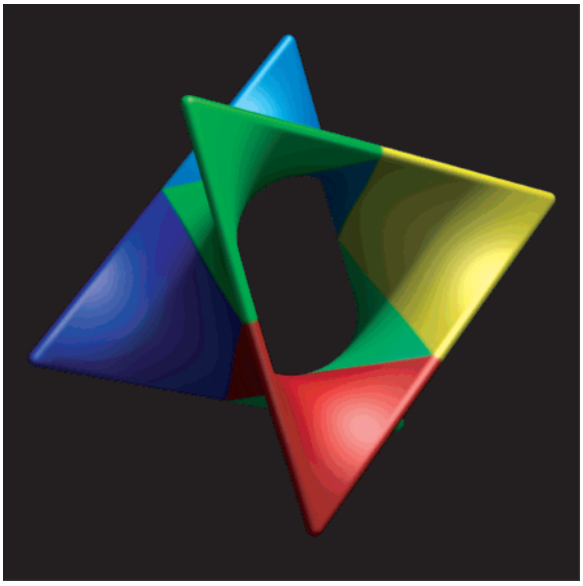

Figure 3. One unit cell of the infinite periodic minimimal surface describing the diamond phase. The six identical surface pieces used to generate the starting configuration are colored differently.

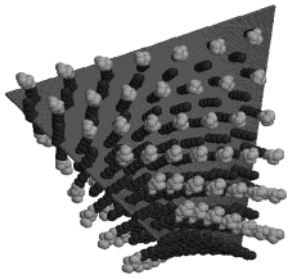

Figure 4. One surface piece with 42 surfactants in each monolayer used as a building block to create the starting structure. Note the surfactants are all trans (except around the double bond), and are fully interdigitated.

From the experimentally determined[18] size of the unit cell (7.4 ± 0.1 nm) at a water ratio of 0.259 ± 0.003 (w/w) the total amount of surfactants per unit cell can be computed, assuming an overall density of 1.0 g/cm^3. (Given the experimental uncertainties in unit cell size and water/surfactant ratio a more accurate estimate based on specific volumes is unnecessary.) Using these quantities, the number of surfactants per unit cell equals 500 ± 20, or 250 ± 10 per monolayer. To determine the positions of the surfactants on a single surface piece as depicted in Figure 3, we discretely solved eq 1 for z on the interval $\{x, y\} \in [0, \pi/2]$ and $\{z\} \in [\pi/2, \pi]$, which describes one surface piece that is oriented, on average, parallel to the xy plane. The xy grid spacing was chosen such as to obtain 6 grid points in one direction, and 7 grid points in the other, producing a total of 42 points. For six surface pieces this amounts to 252 surfactants per monolayer, within the experimental bounds.

In the next step of the procedure the GMO molecules were projected along the normal vectors of the IPMS. The normal vectors of the diamond IPMS are easily derived from the partial derivatives of eq 1.

As a starting surfactant configuration we chose an all-trans conformation (except for a kink at the unsaturated dihedral). This was necessary to avoid initial overlap between neighboring surfactants. A second set of normal vectors was computed between the grid points, and projected toward the opposite site, to generate a bilayer structure. The result of this operation for one surface piece is shown graphically in Figure 4. It shows a nearly homogeneous distribution of the

(16) Mariani, P.; Luzzati, V.; Delacroix, H. *J. Mol. Biol.* **1988**, *204*, 165.
(17) Hyde, S. *Langmuir* **1997**, *13*, 842.
(18) Briggs, H. C. J.; Caffrey, M. *J. Phys. II Fr.* **1996**, *6*, 723.
(19) Schwarz, H. *Monatsch. Berlin. Akad.* **1865**, *3* (27).
(20) Schnering, H.; Nesper, R. *Z. Phys. B* **1991**, *83*, 407.

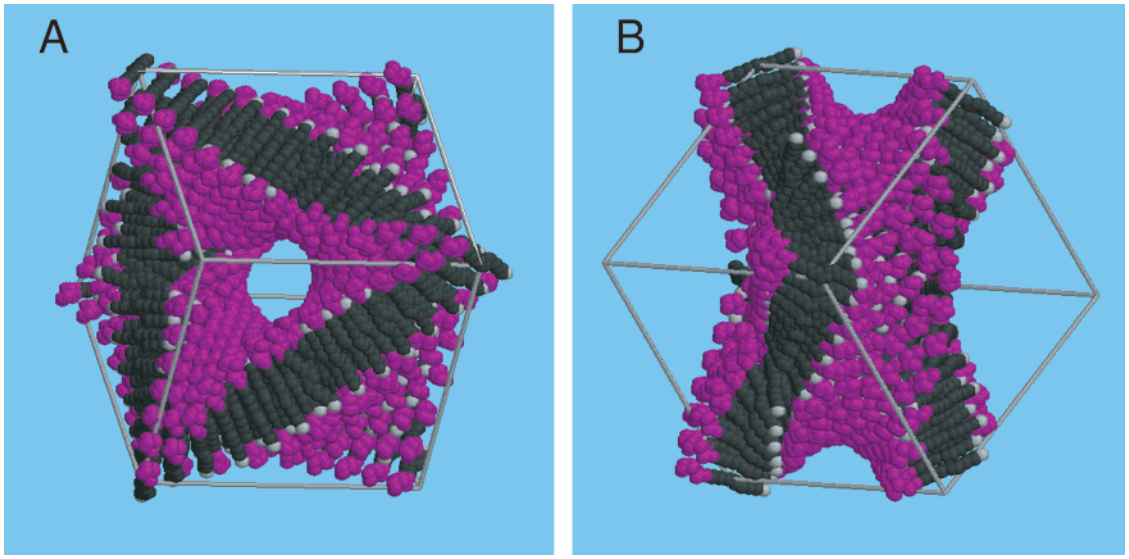

Figure 5. Starting configuration containing 496 GMO molecules in one unit cell of the diamond cubic phase. Water is omitted for clarity. GMO headgroups are colored pink, GMO tails dark gray, and terminal methyl groups light gray. Two separate views are presented to highlight the complicated spatial arrangement.

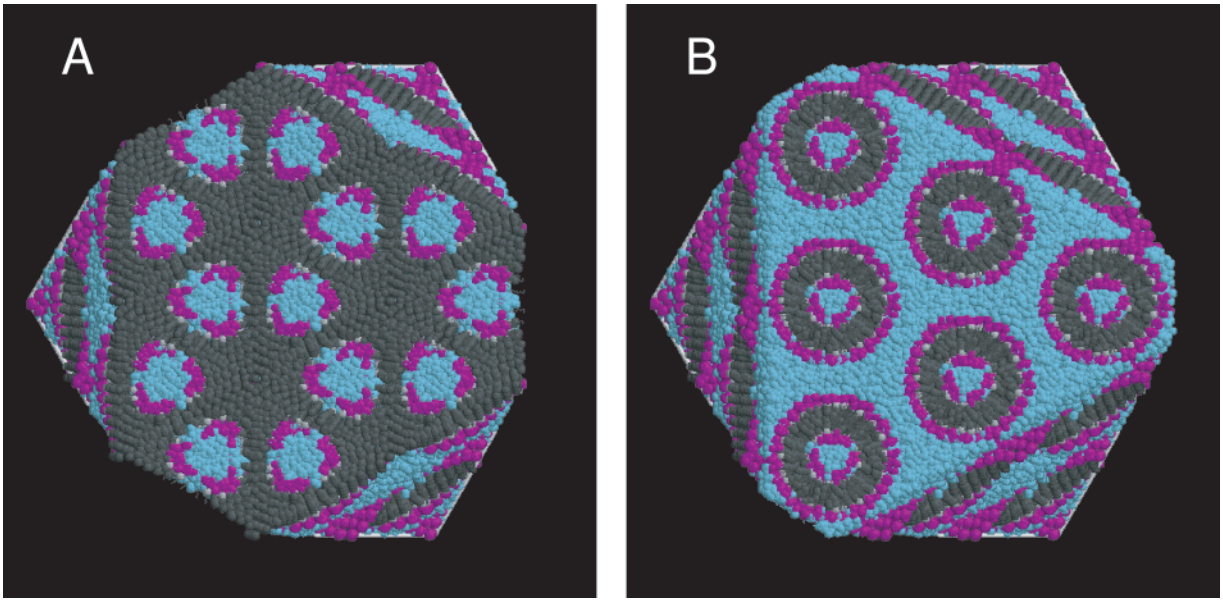

Figure 6. Space-filling image of the starting structure, created by 27 copies of the unit cell displayed in Figure 5. Water molecules are in blue. To illustrate the connectivity of the cubic phase, two different cuts through the system are shown. See text for details.

surfactants across the diamond surface. Note that the surfactants on both sides are interdigitated (see also Figure 5). This was necessary to reduce the total thickness of the bilayer—otherwise the allowed volume for the water became too small. Experimentally the degree of interdigitation is unknown, but it will adjust in the simulation.

The following step involved the application of the symmetry operations to the surface piece to generate the full diamond phase unit cell. Subsequently, the remaining volume was filled with water molecules, using a simple distance criterion based on the vdWaals radii of the atoms. A total number of 3503 water molecules was added, yielding a water ratio of 0.260. This system, containing 504 surfactants and 3503 water molecules, will further be referred to as system I. This water/surfactant ratio did not produce a stable cubic phase (see below). Therefore we also generated a number of starting structures with slightly larger water/surfactant ratios by either randomly removing surfactants or adding more water (starting with a slightly larger initial box volume). System II contains 496 GMO and 3612 water molecules (ratio 0.269), system III 496 GMO and 3744 water molecules (ratio 0.276), and system IV 472 GMO and 3612 water molecules (ratio 0.279).

One of the starting structures (system II) is displayed in Figure 5. Two different orientations are displayed to show the complicated curved nature of the diamond cubic phase. To get a better feeling of the geometry of the diamond phase membrane, we also generated an image of 27 unit cells arranged periodically, using the same starting structure. Two different cuts through this system are shown in Figure 6. The best way of understanding the diamond phase is to view it as a multilamellar bilayer system (look at the sides of the system in Figures 2 and 6) with all the lamellae being connected to each other by toroidal cross connections. Figure 5b shows the toroidal connection in the unit cell. The inside of the toroidal connection forms a water channel (Figure 5a). A cross section through the water phase separating the lamellae (Figure 6B) cuts right through the toroidal cross connections, resulting in circular bilayers arranged in a triangular pattern. A cross section through one of the lamellae (Figure 6A) shows a hexagonal pattern of water channels through the membrane. In an infinite cubic phase two separate intervening water channel networks exist. The water layer between two lamellae has no connection to the water layer directly underneath, but through the toroidal channels to the subsequent water layer and so on.

2.2. Simulation Procedure. All simulations were performed with the Gromacs software (version 2.0).[21] The force field of the GMO molecules is the same as that used for our studies of GMO bilayers,[22]

which is based on the standard Gromacs force field[21] with the headgroup charge distribution taken from Wilson and Pohorille.[23] All atoms are explicitly modeled, except for the hydrogens attached to carbon atoms, for which a united atom model was employed. All bond lengths and all angles involving the headgroup hydrogens were constrained using the Lincs algorithm.[24] The SPC (Simple Point Charge) model was used for the water molecules.[25] Due to the stability of the Lincs algorithm,[26] and the absence of high frequencies, the integration time step was set to 5 fs. A group based twin range cutoff scheme was used to treat the nonbonded interactions. The absence of long-range electrostatic interactions (the charge distribution of the GMO headgroup is not very polarized) allowed a cutoff of 1.0 nm for the Lennard-Jones and of 1.5 nm for the electrostatic interactions. The temperature was kept at 335 K with use of the Berendsen thermostat.[27] Except for the first part of the equilibration procedure (see below), the system was coupled to a constant pressure bath of 1 atm, using isotropic coupling (i.e. all box dimensions change equally).[27] One unit cell of the diamond membrane phase was explicitly simulated, and periodic boundary conditions (PBC) were used to generate a quasi-infinite phase. An interesting consequence of using PBC conditions in the diamond geometry is the possibility for the surfactant molecules to diffuse through the simulation box ending up in the opposite monolayer. In realistic systems this would require flip-flopping that is much slower than diffusion across the simulation box. Given the equality of the two monolayers in the diamond phase this does not constitute a problem. Another peculiarity of the PBC applied to the diamond unit cell as displayed in Figure 5 is the connection of the two water channel networks, destroying their independency. This could only be resolved by simulating a double unit cell (or any even number of copies) which would make the system too large for current simulations. As for the apparent flip-flopping, given the equivalence of the water channel networks we do not expect this PBC effect to be important, however.

The starting configuration was first energy minimized, using a steepest descent relaxation of close atom−atom contacts followed by a short 5 ps MD simulation at constant volume with a time step gradually increasing from 0.1 to 5 fs. This was followed by a 5 ps simulation at constant pressure to allow the overall density to relax. Due to the artificial way of generating the starting structure, the system is still in a highly stressed state. Therefore a series of restrained molecular dynamics (RMD) runs was performed to let the system equilibrate in a controlled manner. Four subsequent 2.5 ns constant pressure simulations were performed with harmonic position restraints put on carbon C4 (see Figure 1). The first RMD run was performed with a strong harmonic coupling constant of $K = 1000$ kJ mol^{-1} nm^{-2}, allowing the surfactant tails to approach their trans/gauche equilibrium distribution and the water molecules to relax while preserving the local interfacial structure. In the following runs the harmonic coupling constant was stepwise diminished to $K = 100$, 10, 1 kJ mol^{-1} nm^{-2}. Each of these runs used the final coordinates of the previous run as the reference restraining coordinates. With $K = 1$ kJ mol^{-1} nm^{-2} the system is only globally constrained, with headgroup motions of 2 nm possible at an energy cost of the order of *kT*.

The original system, system I, already started to deviate from a perfect cubic structure during the weakly restrained MD simulations. One of the water channels started to become drained, producing a contact between the opposite bilayers. Removing the constraints the cubic phase further destabilized during a 5 ns constant pressure MD run. Out of curiosity we nevertheless extended the simulation to see what final equilibrium phase we would obtain. After approximately 35 ns we found the system to have reached an inverted hexagonal phase that remained stable until the end of the simulation at 50 ns. The cubic-hexagonal phase transition is in itself an interesting one, as it is believed to proceed via the biologically relevant stalk mechanism.[12] We will present a detailed analysis of this simulated transition in a forthcoming paper. The aim of the current paper, however, is to describe the properties of a cubic phase. The first modification we tried was a change in the procedure of preparing the starting configuration. Instead of the highly interdigitated structure as displayed in Figures 4 and 5, we generated a partly interdigitated structure. This approach produces less initial stress inside the bilayer, at the cost of more stress in the water phase. The method of creating the starting structure, however, did not affect the stability of the cubic phase. The differences between the starting structures disappeared during the restrained dynamics runs. We also tested the effect of the use of a cutoff for the electrostatic interactions. Employing lattice sums to take into account the long-range, electrostatic interactions appeared to have no effect on the stability of the cubic phase, however. The subsequent modifications we made are all based on the observation that the system eventually relaxed to an inverted hexagonal phase. Inverted hexagonal phases are usually formed by surfactants that have a relatively small headgroup and a large tail volume, inducing a strong negative curvature required for the inverted hexagonal phase. Experimentally,[18] GMO forms a stable single inverted hexagonal phase at high temperatures (365 K) and lower hydration (around 0.2 w/w water ratio) only. High temperatures increase the tail disorder and thereby the tail volume, and low hydration reduces the relative size of the headgroups. Both effects enhance the preference of the surfactants toward negative curvature. To stabilize the cubic phase over the inverted hexagonal phase we performed simulations using the same protocol as sketched above, either at a lower temperature ($T =$ 300 K) or at an enhanced water/surfactant ratio (systems II−IV). The lower temperature run did not show any signs of improvement, and was abandoned after the weakly restrained MD runs. Systems II and IV, however, remained in a stable cubic phase throughout the RMD runs, and still maintained a cubic structure after a 5 ns extended simulation with $K = 1$ kJ mol^{-1} nm^{-2}. Unconstrained MD simulations of 5 ns on both systems did show signs of a slow destabilization (i.e. draining of one of the water channels), although the surfactant geometry remained cubic. System III, with the largest total content, proved to be less stable than systems II and IV.

All the results that will be presented are based on the analysis of the 5 ns extended simulation of the very weakly constrained ($K = 1$ kJ mol^{-1} nm^{-2}) simulation of system II, which is closest in terms of composition to the originally devised system I. This system can be considered to be equilibrated. Both global properties such as the total energy and local ones such as the atom density distributions do not show any significant drift. We argue that the weak constraints do not effect the local organization of the surfactants within the cubic phase, recalling our earlier statement in this section that movements up to 2 nm (in any direction) are allowed at no significant energetic cost. For comparison, we also extended one of the GMO bilayer simulations as described elsewhere.[22] We chose a bilayer containing 800 GMO surfactants, at a fixed area of 0.37 nm^2 which has a bilayer thickness comparable to the bilayer thickness in the cubic diamond phase (see Results). The temperature was set to $T = 335$ K in order to match the temperature of the cubic phase. (Note that the PBC will ensure that the surfactants remain in a lamellar state.)

2.3. Data Analysis. The relative complexity of a cubic membrane compared to a lamellar system makes the analysis of the simulation results far from trivial. Two different types of analysis are needed. One type deals with the over-all organization of the surfactant and water phase within the system, and another type deals with the local arrangement of the individual molecules. The over-all organization is best described in terms of average densities. In our analysis of the cubic membrane we divide our system into an arbitrary number of cubic voxels. For each of the voxels the local mass density of specific atoms, or groups of atoms, is computed. To remove short time and length scale fluctuations, voxel sizes can be changed, or an average can be

(21) Van Der Spoel, D.; Van Buuren, A. R.; Apol, E.; Meulenhoff, P. J.; Tieleman, D. P.; Sijbers, A. L. T. M.; Hess, B.; Feenstra, K. A.; Van Drunen, R.; Berendsen, H. J. C. *Gromacs User Manual*, version 2.0; Nijenborgh 4, 9747 AG Groningen, The Netherlands. Internet: http://rugmd.chem.rug.nl/gmx, 1998.

(22) Marrink, S. J.; Mark, A. *J. Phys. Chem. B* **2001**, *105*, 6122.

(23) Wilson, M. A.; Pohorille, A. *J. Am. Chem. Soc.* **1994**, *116*, 1490.

(24) Hess, B.; Bekker, H.; Berendsen, H. J. C.; Fraaije, J. G. E. M. *J. Comput. Chem.* **1997**, *18*, 1463.

(25) Berendsen, H. J. C.; Postma, J. P. M.; Gunsteren, W. F.; Hermans, J. Interaction models for water in relation to protein hydration. In *Intermolecular Forces*; Pullman, B., Ed.; Reidel: Dordrecht, The Netherlands, 1981; pp 331−342.

(26) Feenstra, K. A.; Hess, B.; Berendsen, H. J. C. *J. Comput. Chem.* **1999**, *20*, 786.

(27) Berendsen, H. J. C.; Postma, J. P. M.; Van Gunsteren, W. F.; Dinola, A.; Haak, J. R. *J. Chem. Phys.* **1984**, *81*, 3684.

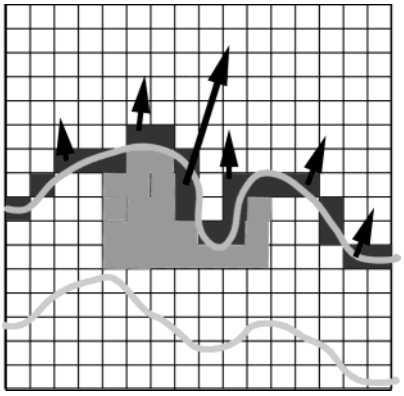

Figure 7. Two-dimensional example of the grid-based method for computation of local surface normals. The two interfaces bordering the bilayer are represented by the two curved lines. The voxels representing one of the surfaces are colored dark gray. The vectors represent the local surface normal vectors. For one surface point (with the big arrow) the subgrid of occupied points is shown that determines the direction of the vector.

taken over subsequent time frames. Comparing local densities, interfacial voxels can be assigned that border regions of high and low density. For instance, the interface between the surfactant phase and the water phase is determined by the set of voxels which contain a comparatively higher surfactant density ("occupied") and which border voxels with a comparatively lower surfactant density ("unoccupied").

The local organization of the surfactants is quite complicated to quantify. In a lamellar system, quantities such as order parameters, or density across the membrane, can be computed easily as the running coordinate is fixed, namely the coordinate perpendicular to the membrane plane. For a nonlamellar system this is not straightforward. If a geometrical expression (like the one given by eq 1) constitutes the true midplane of the membrane, one could define the running axis locally as the vector perpendicular to the geometrical surface. For the cubic phase, however, these expressions are probably only approximations, and the true equilibrium position of the membrane midplane is unknown, although we will show that they approximate the IPMS rather well. Without making any assumptions about the local geometry of the system, however, we calculate the local bilayer normal from the geometry of the interface between the surfactant and water phases. Using the procedure described above, we select the voxels that belong to the interface. For each of these voxels we identify the subgrid of neighboring "occupied" voxels. For this subgrid of occupied voxels a principal component analysis is performed, where voxels more distant from the central voxel are given less weight (using a r^{-2} dependence). The shortest principal axis will be directed perpendicular to the local surface normal. The size of the subgrid determines the variance of the surface normal. Large subgrids probe the curvature of the bilayer globally, producing slowly varying surface normals, whereas small subgrids probe it more locally resulting in large changes over small length scales. Repeating this procedure for all the surface voxels, each of them gets assigned a local surface normal. For nonsurface voxels, the local director was determined by the surface normal of the nearest surface voxel. The method of computing the local surface normals is illustrated in Figure 7. Unless otherwise stated, the results that will be presented in the next section are based on voxel sizes of 0.2 nm cubed, and subgrids of 1.6 nm cubed. Time averages of 100 ps were used to determine the voxel densities. This choice of parameters provided accurate results for lamellar bilayers for which we could compare to standard analysis methods using the perpendicular axis as a director. For the cubic membrane, these parameters suppress the small time- and length-scale fluctuations whereas they preserve the global structure. However, the results do not qualitatively depend on the choices within a reasonable range.

Some of the other properties that characterize lamellar surfactant systems, such as the volume per surfactant, the average number of gauche angles, or the long time diffusion constants can be calculated straightforwardly, as their analysis is independent of the over-all geometry.

3. Results

As discussed in the Simulation Procedure section, the results we present in this section are based on the extended 5 ns weakly constrained simulation of system II, containing 496 GMO and 3612 water molecules. Similar results were obtained for system IV, containing 472 GMO and 3612 water molecules. The global structure is first described, with the emphasis on the difference between the simulated structure and the idealized starting structure based on the IPMS. The subsequent section concentrates on the local organization of surfactant and water compared to their organization in a lamellar bilayer.

3.1. Overall Structure. The final structure of system II is displayed in Figure 8. To facilitate the interpretation, a space-filling representation is given based on 27 copies of the simulation cell. The same cross sections are shown as for the starting structure in Figure 6. Comparing the final structure to the starting structure it is clear that the disorder has increased. The interface between the aqueous and surfactant phase has roughened considerably, and the surfactant tails have melted and adopted a fluid-like structure. The strong triangular nature of the pores in the starting structure seems to have relaxed somewhat into a more spherical shape. To judge how close the center of the bilayer remains to the IPMS, we computed the average local density of the four terminal methylene/methyl groups of the surfactant tail. The average was taken over the whole 5 ns trajectory. This density is displayed as a color map in Figure 9 for several cross sections through the simulation cell. The location of the IPMS is also shown. The center of the bilayer coincides with the IPMS to a large extent. Note that this is not an obvious consequence of the weak constraints—the constraints act on the C4 atoms of the GMO headgroup, whereas the tails are completely free to reorient. The initial location of the tail ends of the surfactants in the starting structure was close to the headgroups rather than in the bilayer center, their final position.

The final unit cell dimension of system II is 7.45 nm, only slightly larger than the experimental value of 7.4 nm that we used to generate the starting structure. The surfactant volume, assuming a volume of 0.03 nm^3 per water molecule, is 0.615 $\pm$ 0.005 nm^3. For our bilayer simulations we find a volume per surfactant of 0.610 $\pm$ 0.005 nm^3, which is identical within the error bounds. The surface area of the GMO molecules is computed by generating a density map of the system as described in the Methodology section. We find a surface area per surfactant of 0.29 $\pm$ 0.02 nm^2 were the error bound reflects the uncertainties due to the parameters used in the analysis. (The variation in surface area between different 100 ps time windows is much smaller.) Note that this surface area really denotes the average area available at the surfactant/water interface. Due to the geometry of the cubic phase the average area available increases along the surfactant tail toward the center of the bilayer. Given the close spatial proximity of the bilayer center to the IPMS (Figure 9) we can calculate the local area $A(z)$ at an arbitrary distance z away from the IPMS using the following equation[28]

$$A(z) = A_0 a^2 + 2\pi\chi z^2 \qquad (2)$$

where $A_0 a^2$ is the area of the IPMS inside a unit cell of size a and χ represents the Euler characteristic of the surface. For a diamond surface, $A_0 = 1.919$ and $\chi = -2$.[28] Using the value

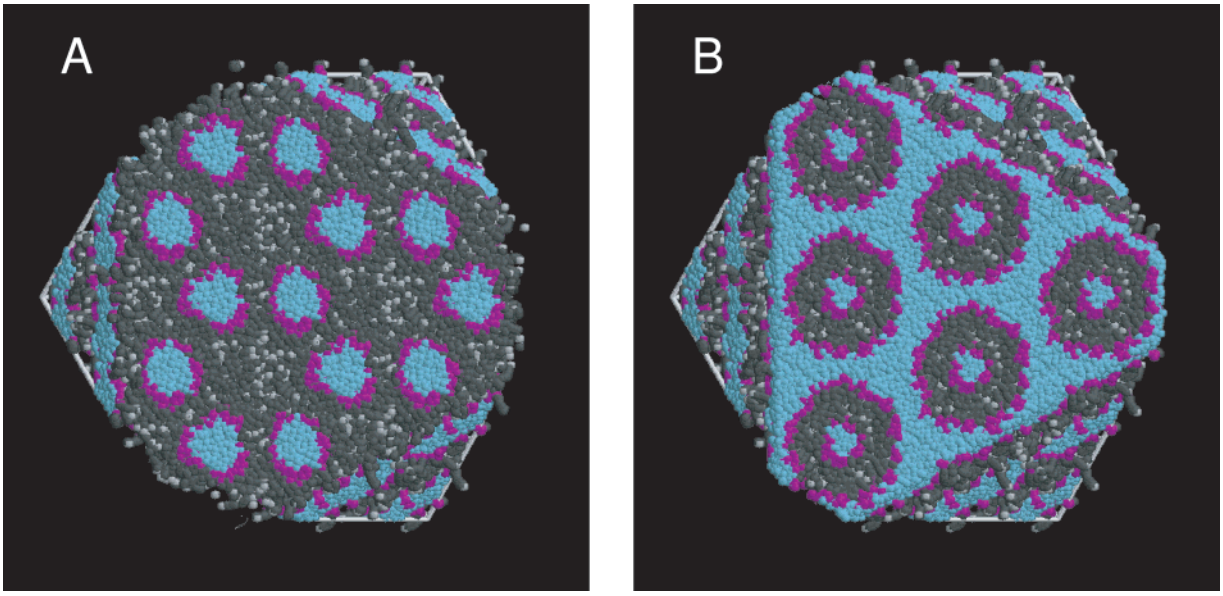

Figure 8. Space-filling image of the final structure, created by 27 copies of the unit cell. The color scheme is the same as in Figures 5 and 6.

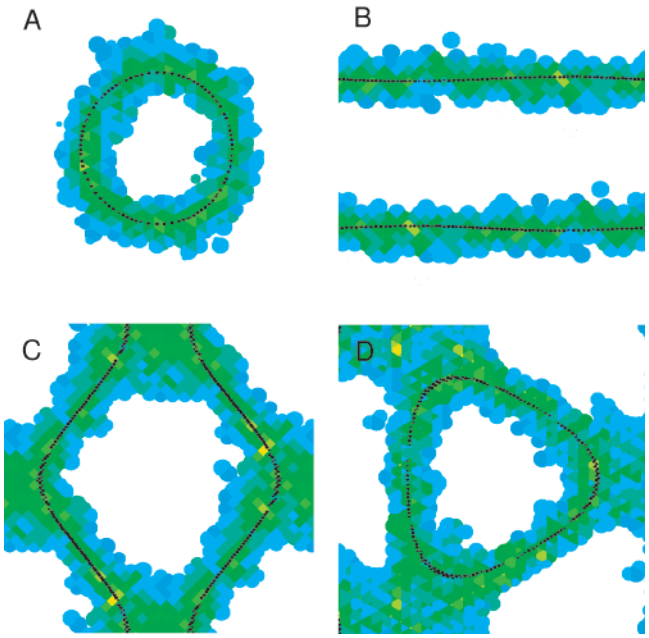

Figure 9. Average density map of tail methyl/methylene groups. Four different slices of the system are shown. Densities are colored yellow-green-light blue-blue-white from high to low. The IPMS is shown in black.

of $a = 7.45$ nm from our simulation, eq 2 predicts an area per surfactant of $A(0) = 106$ nm^2, or 0.42 nm^2 expressed as area per surfactant, at the bilayer center (i.e. $z = 0$). The area that we find for the interface corresponds to a distance of $z = 1.6$ nm, implying a bilayer thickness of 3.2 nm. This is equal to the thickness of the lamellar bilayer, which has a surface area of 0.37 nm^2 (see Simulation Procedure). An equivalent surface area of 0.37 nm^2 for GMO in the cubic phase is found at a distance 1.0 nm away from the IPMS. A similar expression to eq 2 can be derived for the volume $V(z)$ enclosed by the IPMS and a surface at a distance z:

$$V(z) = A_0 a^2 z + \frac{2}{3}\pi\chi z^3 \qquad (3)$$

Substituting the estimated monolayer thickness of $z = 1.6$ nm

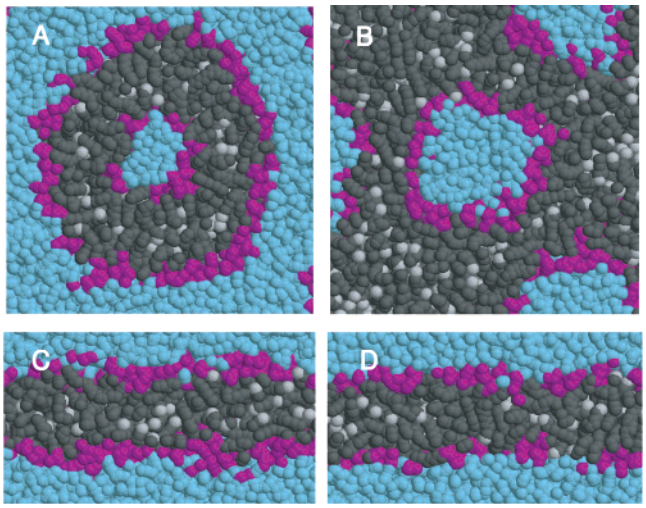

Figure 10. Closeup of local bilayer structure: (A) cross section of the toroidal connection; (B) cross section through the water channel; (C) cross section through the lamellar section. Panels A−C are all snapshots of the cubic phase. (D) Lower right: cross section through the lamellar bilayer phase.

we obtain $V(z{=}1.6) = V_{GMO} = 0.62$ nm^3, close to the more accurate estimate given above. The reverse calculation was done for the experimental system.[18] Assuming equal partial specific volumes for the surfactant and water components, the experimental system closest to the systems simulated has $a = 7.4$ nm and a total surfactant volume $V = 300$ nm^3.[18] The volume for a monolayer is then 150 nm^3, which can be substituted into eq 3 and solved for z. This results in a monolayer thickness of $l = 1.6$ nm, equivalent to our result. We can also use eq 2 to obtain an estimate of the average radius r_w of the water channels, assuming that $A(z) = 0$ at $z = r_w + l$.[18] This expression is valid for a perfect cubic symmetry and predicts $r_w = 1.3$ nm for our case. (The experimental estimate[18] using the same procedure predicts $r_w = 1.5$ nm at 335 K for a fully hydrated diamond phase (0.29 w/w). Our hydration level of 0.269 (w/w) is slightly smaller.)

3.2. Local Structure. In Figure 10 we show closeups of the final configuration of the weakly constrained simulation of system II. The figures illustrate the local bilayer structure of the diamond phase at the simulated state conditions. Figure 10

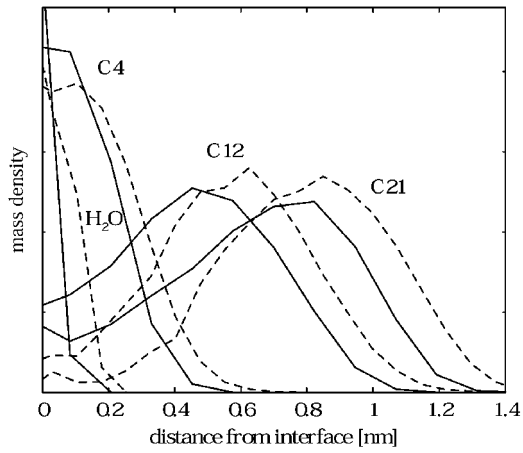

Figure 11. Mass density of atoms across the local bilayer normal. The distance ordinate measures the distance to the nearest interface. Solid lines denote the lamellar bilayer and dashed lines the cubic.

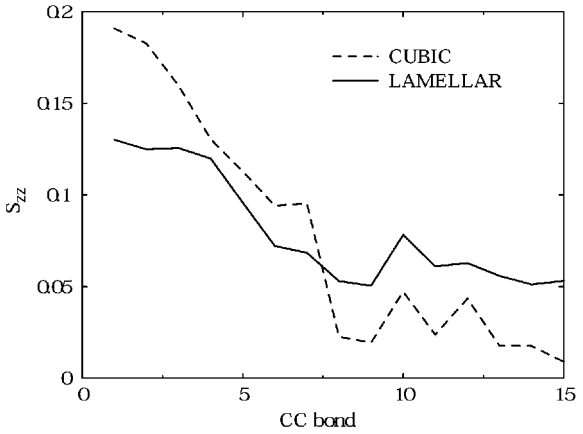

Figure 12. Order parameter with respect to the local bilayer normal as a function of bond position along the surfactant chain (i.e. bond 1 is the bond between C1 and C2, bond 3 that between C3 and O3, bond 5 that between C4 and C5, etc.; the double bond is bond 13). The solid line denotes the lamellar phase and the dashed line the cubic phase.

also shows a snapshot of a GMO bilayer simulated at a surface area of 0.37 nm^2. This particular bilayer area was chosen as it produces a bilayer with a thickness comparable to the thickness calculated for the simulated cubic phase. Inspection of the graphical images in Figure 10 shows the similarity in bilayer thickness. Not only the thickness, but the whole appearance of the local bilayer structure in the cubic phase seems very similar to that of a lamellar bilayer. At the high temperature of the simulations ($T = 335$ K) the surfactant tails of both bilayers are very disordered. The interface seems somewhat more disordered in the case of the cubic bilayer. To quantify the roughness of the interface, we analyzed the scaling of the computed area as a function of the grid size used to compute the phase map (see Methodology section). The dependence of area A on grid size L can be expressed in terms of a roughness exponent $\eta(L)$ as $A \propto L^{2-\eta(L)}$. For a completely flat surface, $\eta = 2$ and the surface area will not depend on the size of the grid to measure it. For a fractal surface, $\eta = d_f$, where d_f is the fractal dimension of the surface. For self-affine systems such as interfaces the roughness exponent will not be constant but depend on the length scale of measuring. Applying this procedure for both our cubic and lamellar bilayer system, we find that at length scales of 1 nm the surfaces are scaling essentially as flat surfaces. On smaller length scales, the roughness exponent starts to increase gradually, until the grid size becomes so small that the concept of an interface breaks down. For meaningful length scales between 0.2 and 1.0 nm the roughness exponent for the cubic phase compared to the lamellar one appears to be consistently larger. For instance at a length scale of 0.6 nm comparable to the inter-headgroup spacing we find $\eta = 2.5$ and 2.3 for the cubic vs the lamellar phase, respectively.

To further compare the local bilayer structure of the lamellar versus the cubic phase, in Figure 11 the atom densities along the local bilayer normal are plotted. The distribution of the displayed atoms is very similar. In agreement with the larger interfacial roughness exponent for the cubic phase, we see a slightly broader distribution of the water and C4 carbon (close to the headgroup, see Figure 2). The position of the interface (equal water and surfactant density) differs by about 0.1 nm. The C12 (double bond) and C21 (terminal methyl) distributions are surprisingly similar to the lamellar distribution but shifted over a similar distance of approximately 0.1 nm. Only the density of tail atoms in the interfacial region is significantly higher in the case of the lamellar phase. Apparently it is easier for the GMO molecules in the lamellar bilayer phase to backfold, which is explained by the larger interfacial surface area of the lamellar phase with respect to the cubic phase. We also analyzed the possibility of interdigitation in the equilibrium structures by comparing the distribution of the C21 atoms to C20 and C19, but found that the distance to the interface for the maximum of the C21 peak was largest, indicating no average interdigitation. This is equally true for both the lamellar and cubic phases.

In Figure 12 the order parameters are presented. Like the atom densities, the order parameters are calculated with respect to the local surface normal as explained in the Methodology section. Compared to the lamellar bilayer, the ordering of the C−C bonds in the cubic phase is clearly higher toward the interface, and clearly lower toward the center of the bilayer. The order parameters reflect the locally available area per surfactant in the cubic phase, with relatively high order at the low area region near the interface, and low order near the center of the bilayer where the area is large. The same trend is seen in the average fraction of trans dihedrals. Dihedrals close to the headgroup have a trans fraction of 0.75 in the cubic phase, compared to 0.7 for the lamellar phase. For the dihedrals near the surfactant tail ends, the trans fraction is 0.6 for the cubic phase versus 0.65 for the lamellar phase.

Finally we analyzed the diffusion constant for the water molecules from their mean-square displacement (MSD) in time. The MSD is calculated averaging over all the water molecules in the system, irrespective of their position. For isotropic systems the diffusion constant is obtained from the long-time limit of the MSD, i.e., $D = \lim_{t\to\infty}(\langle\{r(t) - r(0)\}^2\rangle/2dt)$, where d is the dimensionality. The MSD for water in the cubic phase and in the lamellar phase (split into lateral and perpendicular displacement) are presented in Figure 13. Each of the three MSD curves shows typical behavior. The lateral displacement of the water molecules in the lamellar phase is linear with time over the whole range, with a diffusion constant of $D = 6.7 \pm 0.1 \times 10^{-5}$ cm^2 s^{-1}, which is equal to the diffusion constant of bulk SPC water (at 335 K).[29] The lateral diffusion of the interlamellar water thus proceeds unhindered. In the perpendicular direction this can obviously not be the case, which is seen in the leveling off of the MSD curve. The water molecules become trapped at

(28) Anderson, D.; Gruner, S.; Leibler, S. *Proc. Natl. Acad. Sci. U.S.A.* **1988**, *85*, 5364.

(29) Postma, J. P. M. MD of H_2O. A Molecular Dynamics Study. Ph.D Thesis, University of Groningen, 1985.

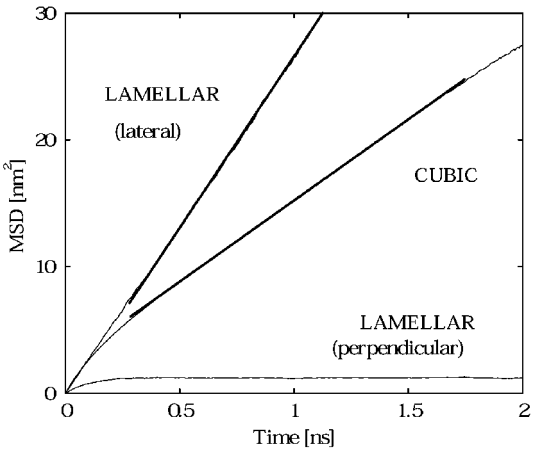

Figure 13. Mean square displacement of water molecules as a function of time. The solid line denotes the lamellar phase and the dashed line the cubic phase. The lamellar MSD is split into lateral and perpendicular contributions. The bold lines indicate linear fits from which the diffusion constant is calculated.

time scales larger than a few hundred picoseconds, and their displacement will be limited by the interlamellar spacing (≃1 nm in the lamellar simulation). The effective long time diffusion constant in the perpendicular direction therefore is zero. Within the cubic network of water channels we have an intermediate situation. On short time scales the water molecules experience an anisotropic environment due to the cubic surfactant phase. On large time scales, however, the system appears isotropic and a linear MSD in time is observed. The crossover toward isoptropic diffusion occurs at a time scale of roughly 0.5 ns, or at an average displacement of 3 nm. This corresponds to the length scale of one of the flächenstücke, which is the basic building unit of the cubic phase. Beyond this length scale the cubic system appears isotropic. The long-time diffusion constant in the cubic phase is $D = 2.1 \pm 0.1 \times 10^{-5}$ cm^2 s^{-1}, which is about a factor of 3 smaller than the diffusion constant of bulk water. Note that this is an effect of the topology of the cubic matrix, and not due to interactions of water and surfactant molecules, otherwise we should have observed a slowing down of the lateral diffusion in the lamellar system. The calculated factor of 3 is in very good agreement with experimental results for diamond phases[30] which predict a ratio of $D/D_{bulk} \simeq 0.3$ for a range of systems including monoolein.

4. Discussion

Although the weak constraints allowed quite large movements of individual surfactant molecules, when we released the constraints we were not able to stabilize the cubic phase. Collective effects probably drive the phase transition toward the inverted hexagonal phase as we observed in one of our extended simulations (which will be reported elsewhere). There are a number of reasons that could explain the apparent instability of the cubic phase in our simulation. First of all the force field and simulation parameters might not be accurate enough to simulate a stable cubic phase. The fact that these parameters are successfully used in simulations of lamellar and micellar structures does not automatically guarantee their applicability to cubic phases. It is likely that the balance of the forces that drive aggregation into a cubic phase is very subtle. Experimentally it is known that the enthalpy change going from a cubic to an inverted hexagonal phase is only small (about 1 kJ/mol[31]), and that the diamond phase of GMO is stable in a narrow temperature/composition range only.[18] Another possible reason for the difficulty stabilizing the cubic phase is the fact that the geometry of the unit cell is fixed. The use of isotropic pressure scaling (required for a cubic geometry) allows the total density to relax, but the system does not have the possibility for instance of swelling. Given the uncertainty in the experimental determination of the unit cell size and composition, this could pose a serious problem. Note that in the case of lamellar bilayer simulations the system does have the ability to change the lipid area, and therefore to swell, if nonisotropic pressure scaling is applied. A third cause of destabilization could originate from the fact that we used periodic boundary conditions on a single unit cell. As explained in the methodology, these conditions connect the two water channel networks that exist in an infinite cubic phase. It is therefore worthwhile to try to repeat the current simulations for a double unit cell soon. The way of generating the starting structure could in principle be another factor influencing the stability of the cubic phase. Given the careful way in which we let the system equilibrate, and given the convergent results we got using either more or less interdigitated starting structures, this seems less likely.

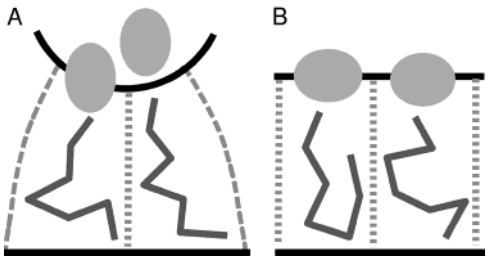

Figure 14. Schematic model of surfactant packing in cubic (A) versus lamellar bilayers (B). For clarity, the differences are exaggerated.

Increasing the water/surfactant ratio slightly we were able to perform stable simulations of the cubic diamond phase under weakly constrained conditions. This proves that we are at least quite close to a stable phase, and therefore we assume that our results reflect the properties of an equilibrium diamond cubic phase. One of the main assumptions about cubic phases of the inverse type is that the bilayer midplane is close to the IPMS. Our results show that this assumption is very realistic. Apart from small fluctuations we did not find any systematic deviations of the peak density of the surfactant tail ends from the IPMS. Based on this assumption we estimated surfactant volume, monolayer thickness, and average water channel radii in close agreement with the experimental system. Given the packing constraints within the cubic phase, however, there is not much room for large discrepancies as long as the cubic symmetry is maintained.

More interestingly, the simulations allowed us to analyze the local organization of the surfactants within the diamond phase. Based on our results we propose a model for the organization of the surfactants in the cubic bilayer phase compared to a lamellar bilayer phase. This schematic model is shown in Figure 14. The left side shows the packing of the surfactants in the cubic phase. The right side shows the packing of a surfactant in a lamellar bilayer phase with an equivalent lipid volume and similar bilayer thickness. Note that the figure exaggerates the differences in surfactant packing. Bear in mind however that our results show the overall structure of the surfactants in both phases to be rather similar. Focusing on the differences, the negative curvature of the cubic phase implies a smaller surface

(30) Lindblom, G.; Rilfors, L. *Biochim. Biophys. Acta* **1989**, *988*, 221.

(31) Hyde, S.; Andersson, S.; Ericsson, B.; Larsson, K. *Z. Kristallogr.* **1984**, *168*, 213.

area in the headgroup region. As our results on the atom distributions plus the analysis of the roughness exponent show, this tension is released by allowing more perpendicular freedom of the headgroups. (Figure 14 might seem to imply a completely smooth packing of headgroups in the lamellar phase. This is of course not realistic. The degree of disorder is, however, clearly larger for the cubic phase.) The order parameter profile indicates a concomitant increase in headgroup orientation perpendicular to the membrane plane, and an increase in chain order in the region closest to the headgroups. Toward the bilayer center, the available volume in the cubic phase increases, and the chain order becomes less compared to the lamellar phase. Another consequence of the increased volume is the less frequently observed backfolding of the surfactant tails. This is shown by the density profiles of the tail groups. In both the lamellar and cubic bilayer the largest density of tail groups is found in the middle of the bilayer, however. For the cubic phase the center of the bilayer stays close to the surface defined by the geometric expression for the infinite periodic minimal surface of the diamond phase. It would be interesting to see if this model holds for cubic phases in general, for other cubic geometries, other state conditions, and other types of surfactants. We would finally like to point out that the recognition of a tapered local volume model for the packing of surfactants in an inverted cubic phases is not new (it lies at the heart of structural models using minimal surfaces, e.g., refs 31 and 32). As we have shown, the details of the packing of surfactants within such a tapered local volume can be revealed by MD simulations.

5. Conclusion

Atomistic simulations of a diamond cubic phase of GMO surfactants have shown that the bilayer midplane is located very close to the infinite periodic minimal surface describing the diamond geometry. The packing of the GMO surfactants within the cubic bilayer structure is similar to that within a lamellar bilayer phase. The constraints imposed by the smaller interfacial surface area in the cubic phase are resolved by a slightly more disordered headgroup region and a larger tendency toward perpendicular packing of the surfactant tails close to the interface. The diffusion rate of water inside the aqueous channels is slowed by a factor of 3 compared to bulk water.

Acknowledgment. The authors acknowledge Peter Nollert and Steve Hyde for helpful discussions. D.P.T. is a Scholar of the Alberta Heritage Foundation for Medical Research; S.J.M. is funded by the Royal Dutch Academy of Science (KNAW).

JA016012H

(32) Hyde, S. *J. Phys. Chem.* **1989**, *93*, 1458.